IEEE Access
Multidisciplinary ⋮ Rapid Review ⋮ Open Access Journal

Received 9 November 2023, accepted 29 November 2023, date of publication 7 December 2023,
date of current version 13 December 2023.

Digital Object Identifier 10.1109/ACCESS.2023.3340204

RESEARCH ARTICLE

A Deep Learning-Based Indoor Radio Estimation Method Driven by 2.4 GHz Ray-Tracing Data

CHANGWOO PYO, HIROKAZU SAWADA, (Member, IEEE), AND TAKESHI MATSUMURA, (Member, IEEE)

Wireless Systems Laboratory, Wireless Networks Research Center, Network Research Institute, National Institute of Information and Communications Technology, Yokosuka 239-0847, Japan

Corresponding author: Changwoo Pyo (cwpyo@nict.go.jp)

This work was supported by the Contract ''Research and Development for the Realization of High-Precision Radio Wave Emulator in Cyberspace'' funded by the Ministry of Internal Affairs and Communications of Japan under Grant JPJ000254.

ABSTRACT This paper presents a novel method for estimating received signal strength (RSS) in indoor radio propagation using a deep learning approach. The proposed method utilizes a training dataset comprised of imitated real-world indoor environments and radio-map images generated through 2.4 GHz ray-tracing. Additionally, we introduce a convolutional neural network (CNN) named Radio Residual UNet (RadioResUNet) to facilitate the training and prediction of indoor radio propagation. To assess the feasibility and effectiveness of this deep learning network for indoor radio estimation, we compare the RSS obtained from practical wireless equipment with that obtained by RadioResUNet in two indoor environments: an anechoic chamber and an office floor. Furthermore, we explore the prediction outcomes achieved using different loss functions, including mean squared error (MSE), binary cross-entropy (BCE), and dice binary cross-entropy (Dice_BCE), across varying dataset sizes. The results reveal that the proposed deep learning-based radio estimation method exhibits estimation discrepancies of 4.25 dB and 5.4 dB compared to practical measurements in real-world environments of the anechoic chamber and the office floor, respectively. These results indicate a performance that is comparable to the indoor propagation model of ITU-R P.1238. Additionally, we introduce an indoor radio estimation tool that utilizes the deep learning network of RadioResUNet to predict radio propagation in a target area with minimal input.

INDEX TERMS Convolutional neural network (CNN), deep learning-based radio estimation, received signal strength (RSS), indoor radio propagation, RadioResUNet, ray-tracing.

I. INTRODUCTION

The widespread adoption of wireless communications in various local fields, including transportation, construction, factories, and medical care, has led to an increasing demand for easy wireless network construction [1], [2], [3], [4]. However, with the coexistence of various wireless systems such as Wi-Fi, Bluetooth, LPWA, 4G, and 5G cellular, as well as the development of new wireless systems of beyond 5G (B5G) and 6G, selecting and applying the optimal wireless system in real-world environments has become a critical issue for achieving high system efficiency [5], [6].

Developers usually plan the placement of multiple access points in specific locations to optimize wireless connectivity for devices when implementing local wireless networks in targeted areas. However, pinpointing the appropriate location for installing these access points can be challenging due to numerous factors that can influence the quality of wireless connections, such as building layout, terminal mobility, and obstructions. For example, a newcomer to the world of wireless communications may plan to set up a Wi-Fi network within their office. While installing a Wi-Fi access point in any location in the office and checking device connectivity may seem like the most straightforward approach, this method is time-consuming and may not guarantee the most optimal connectivity for devices within the office.

A more advanced approach to deploying Wi-Fi networks involves using analytical models to simulate their installations. There are various models, including theoretical, statistical, and simulation-based ones, that can be employed

The associate editor coordinating the review of this manuscript and approving it for publication was Ding Xu.

to estimate the radio environment [7]. Additionally, the wireless emulator project aims to develop a large-scale wireless emulation platform for the high-speed and large-scale verification of emerging wireless communication systems and technologies in a virtual space. The ongoing development of the large-scale wireless emulator represents an approach to speed up evaluations and enable virtual testing of wireless communication systems [8], [9]. While these methods can be helpful for beginners, constructing a model that meets the user's needs requires specialized knowledge, and the applicable wireless parameters must be carefully considered to obtain more accurate results.

Beginners in deploying wireless networks often face difficulties in real-world scenarios and usually rely on the expertise of wireless professionals to evaluate the wireless environment and determine the best location to install access points based on various conditions and requirements. These experts use methods such as theory, statistics, and simulation tools to provide outputs. While this approach can meet user requirements, it can also be costly and time-consuming, as constructing a wireless network involves a substantial amount of trial and error, which must be executed iteratively to achieve the optimal outcome. In the initial stages of deploying a local wireless network, it is crucial to comprehend the wireless environment of the target area, as it can save time and expenses associated with traditional procedures. For beginners, it is important to have an easy understanding of the wireless situation in their desired area without engaging in complex tasks.

In order to meet these requirements, our main contribution is the development of a radio estimation tool that utilizes deep learning, eliminating the need for analytical models or simulation expertise. The tool predicts the wireless environment in the target area by leveraging preprocessed radio propagation data obtained through ray-tracing by professional wireless analysts. With minimal information provided by beginners, the tool simplifies the radio estimation procedure by removing the need to directly handle analytical models.

To realize a tool simplifying radio estimation, this paper presents a novel method for estimating indoor radio propagation using deep learning. The proposed deep learning-based radio estimation method utilizes a training dataset comprising imitated real-world indoor environments and radio-maps generated by ray-tracing. In the context of ray-tracing, a radio-map typically represents a two-dimensional (2D) depiction of radio wave propagation characteristics in a given environment. These radio-maps, generated from ray-tracing simulations, serve as training data for deep learning-based radio estimation.

This paper introduces a simple and large-scale indoor layout modeling method for creating an indoor environment dataset for deep learning. To train and predict indoor radio propagation, a convolutional neural network (CNN) called Radio Residual UNet (RadioResUNet) is introduced in this paper. The feasibility and effectiveness of the proposed deep learning network for indoor radio estimation are verified by comparing the received signal strength (RSS) measured by practical wireless equipment with those obtained by RadioResUNet in indoor environments of the anechoic chamber and the office floor. The results demonstrate the effectiveness of the deep learning network for indoor radio estimation and indicate a performance that is comparable to the empirical indoor propagation model of ITU-R P.1238 [10].

The rest of the paper is organized as follows. Related works are shown in Section II. Section III describes the procedures of deep learning-based radio estimation for indoor environments, and Section IV introduces the proposed deep learning network of RadioResUNet. Estimation and verification results of the proposed deep learning-based radio estimation are shown in Section V. Section VI concludes this paper.

II. RELATED WORKS

Deep learning has been successfully applied in wireless communication systems, including physical layer components and wireless network management [11]. The physical layer of wireless communication systems plays a critical role in transmitting and receiving signals over the air, and optimizing its performance is vital for ensuring high-quality wireless communication. Deep learning techniques have been employed to optimize various physical layer components, such as modulation and coding schemes, power control, beamforming, channel estimation, and equalization [12], [13], [14], [15], [16]. Additionally, a method that employs ensemble learning techniques has been proposed for predicting RSS using unmanned aerial vehicles (UAVs) in mobile communications [17].

Furthermore, deep learning techniques have been applied to improve various aspects of wireless network management, including resource management and network management. Resource management aims to enhance network performance and efficiency by optimizing the allocation and utilization of resources, such as radio spectrum, power, and network resources [18], [19], [20]. On the other hand, network management involves tasks such as monitoring and controlling the network, identifying and resolving network issues, optimizing network topology, and ensuring quality of service [21], [22], [23].

Recent studies have explored the use of deep learning for scheduling and routing in wireless networks, involving the optimization of resource allocation, such as time slots and frequency bands for different users or applications, as well as determining the most efficient routes for transmitting data packets through the network [24], [25], [26], [27].

Convolutional neural network (CNN) is one of the typical deep learning networks used for image classification, recognition, and segmentation [28], [29]. Various image analysis models using CNNs have been proposed. Residual network (ResNet) is a deep learning network that utilizes

the residual block and skip connection method to address the issue of model degradation caused by the vanishing gradient problem in deep learning [30]. UNet is one of the fully convolutional networks (FCNs) developed for pixel classification in medical images, employing convolutional down-sampling and up-sampling techniques [31]. UNet also employs skip connections to retain positional information in images that can be lost during convolutional up-sampling. Residual UNet (ResUNet) is a deep learning network in which a combination of the residual block and skip connections is added to the convolutional layer to facilitate efficient deep learning [32].

Radio-map images generated by ray-tracing can serve as training data for deep learning networks. RadioUNet is an extended network based on UNet, proposed for estimating the outdoor wireless environment through image segmentation of radio-maps calculated by ray-tracing [33]. A framework for a machine learning-based propagation model has been proposed to estimate received signal strength (RSS), considering the physical and geometric structure of the propagation environment in urban cellular networks [34].

III. DEEP LEARNING-BASED INDOOR RADIO ESTIMATION METHOD

In this section, we present a deep learning-based indoor radio estimation method. The method involves creating a training dataset of indoor environments that simulate various real-world settings, along with radio-maps generated by ray-tracing within the environments. We also propose a deep learning network that learns the training dataset to infer the indoor radio propagation.

A. A DEEP LEARNING PROCEDURE

Figure 1 depicts the deep learning procedure used for radio estimation. Firstly, datasets containing images of indoor environments, transmitter positions, and radio-maps are prepared for training and validating the deep learning model. During the recursive training phase, the deep learning model infers radio-maps as prediction results and optimizes training parameters, including the weights and biases of the deep learning model, using a loss function. The estimation results predicted by the pre-trained model are verified by comparing them to wireless equipment measurements in real-world indoor environments.

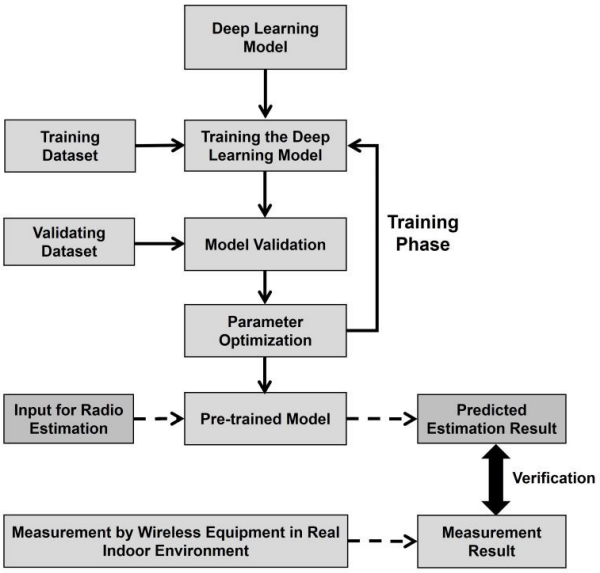

FIGURE 1. A deep learning procedure for radio estimation.

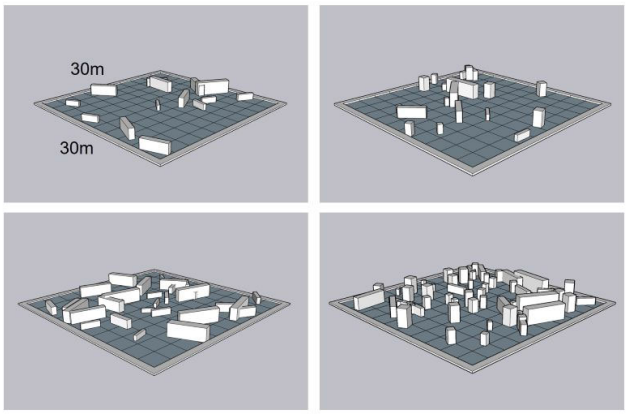

FIGURE 2. Examples of the indoor layout with the different density, where the number and size of objects vary on a 30 m × 30 m plane.

B. DATASETS

To enable deep learning-based radio estimation, we prepare three datasets for training and validating the network: an indoor environment dataset, a transmitter position dataset, and a radio-map dataset.

1) INDOOR ENVIRONMENT DATASET

For deep learning-based indoor radio estimation, it is necessary to train the network on various indoor environments, as radio conditions are highly influenced by the environments. However, creating a dataset that represents a variety of practical indoor environments is challenging due to the diverse layouts and building structures of indoor spaces, which depend on their intended use, such as offices, factories, and auditoriums. This paper introduces a simple and large-scale indoor layout modeling method for creating an indoor environment dataset for deep learning.

Indoor spaces contain various square and rectangular structures such as walls, furniture, doors, windows, and more. To represent indoor environments, we randomly arrange 3D square and rectangular boxes of different sizes on a 30 m × 30 m plane, as shown in Figure 2. We assume that the maximum height of indoor objects is 3 m, and the indoor density and layout may vary depending on the number and size of objects in the space. We create 80 indoor datasets with varying densities (the number of objects per m^2), which form our indoor environment dataset. Figure 2 provides examples of 3D indoor layouts with different densities. We also

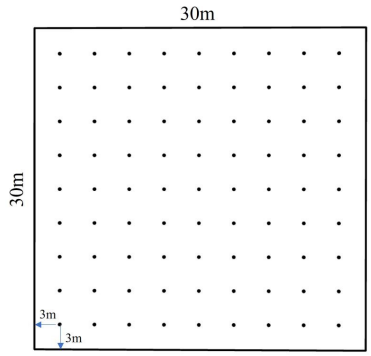

FIGURE 3. Transmitter positions on a 30 m × 30 m plane.

TABLE 1. Ray-tracing parameters for calculating radio propagation.

Parameter	Value
Operation Frequency	2.442 GHz
Transmitter (TX) Power	200 mW
Antenna Pattern	Isotropic Antenna
Transmitter Height	2.5 m
Number of propagation paths	20
Number of penetrations	2
Number of reflections	2
Number of diffractions	1

use these 3D indoor layouts to generate radio-maps using ray-tracing.

To use the created indoor environments in the CNN-based deep learning network, we convert the 3D layouts to 2D images. We slice the 3D layouts at heights of 0.5m, 1.5m, and 2.5m and save each slice as a 2D image for training. We color the sliced rectangular objects using grayscale to represent the blockage of radio propagation, while the space with grayscale of RGB (255, 255, 255, i.e., white) represents open space. The RGB grayscale values for rectangular objects are as follows: metal is RGB (60, 60, 60), concrete is RGB (120, 120, 120), wood is RGB (180, 180, 180), and glass is RGB (240, 240, 240). The default grayscale value for an object without a specified material is RGB (0, 0, 0).

For data augmentation, we rotate the 2D images by 90, 180, and 270 degrees. In total, the indoor environment dataset contains 4800 images generated from 80 indoor layouts, with 3 slices per layout, 4 rotations per slice, and 5 materials per slice.

2) TRANSMITTER POSITION DATASET

The strength of the radio signal is largely affected by the distance between a transmitter and a receiver. To account for this, we place a transmitter at the intersection of a 3 m × 3 m grid on a 30 m × 30 m plane, and prepare 81 transmitter positions as shown in Figure 3.

3) RADIO-MAP DATASET

A radio-map is a 2D image that represents the radio propagation of the received signal strength (RSS) between a transmitter and a receiver. To calculate the radio propagation, we used ray-tracing radio propagation software of WinProp [35] with the parameters: a frequency of 2.4 GHz, a transmitter antenna height of 2.5 m, a transmit power of 200 mW, and isotropic antennas with 0 dBi for both the transmitter and receiver as shown in Table 1. Ray-tracing is a practical method for measuring radio propagation, widely applied in wireless communication environments. This technique provides a comprehensive understanding of

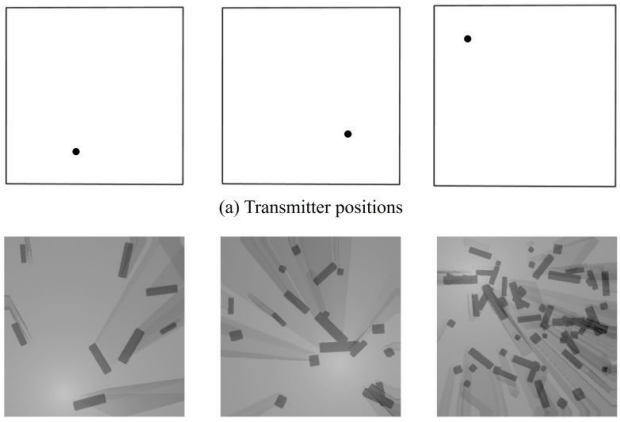

FIGURE 4. Examples of radio-maps generated by ray-tracing from the different indoor layouts and transmitter positions.

RSS			R	G	B	Gray color
~		-26 dBm	255	255	255	
-26 dBm	~	-28 dBm	243	243	243	
-28 dBm	~	-30 dBm	232	232	232	
-30 dBm	~	-33 dBm	221	221	221	
-33 dBm	~	-36 dBm	210	210	210	
-36 dBm	~	-39 dBm	200	200	200	
-39 dBm	~	-42 dBm	190	190	190	
-42 dBm	~	-45 dBm	180	180	180	
-45 dBm	~	-48 dBm	171	171	171	
-48 dBm	~	-51 dBm	162	162	162	
-51 dBm	~	-54 dBm	153	153	153	
-54 dBm	~	-57 dBm	145	145	145	
-57 dBm	~	-60 dBm	137	137	137	
-60 dBm	~	-63 dBm	129	129	129	
-63 dBm	~	-66 dBm	121	121	121	
-66 dBm	~	-69 dBm	114	114	114	
-69 dBm	~	-72 dBm	107	107	107	
-72 dBm	~	-75 dBm	100	100	100	
-75 dBm	~	-78 dBm	93	93	93	
-78 dBm	~	-81 dBm	86	86	86	
-81 dBm	~	-84 dBm	79	79	79	
-84 dBm	~	-87 dBm	72	72	72	
-87 dBm	~	-90 dBm	65	65	65	
-90 dBm	~	-93 dBm	58	58	58	
-93 dBm	~	-96 dBm	51	51	51	
-96 dBm	~	-99 dBm	44	44	44	
-99 dBm	~	-102 dBm	36	36	36	
-102 dBm	~	-105 dBm	27	27	27	
-105 dBm	~	-108 dBm	16	16	16	
-108 dBm	~		0	0	0	

FIGURE 5. RGB values for grayscale representing receiver signal strength (RSS).

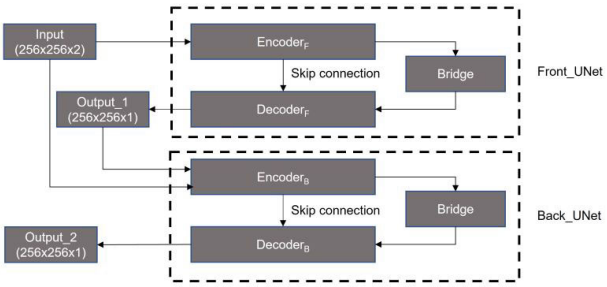

FIGURE 6. Overview of RadioResUNet.

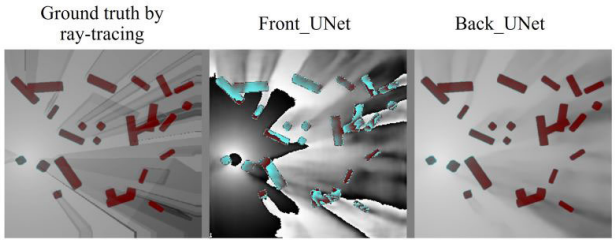

FIGURE 7. Predicted output examples of Front_UNet and Back_UNet for the ground truth image.

how radio waves interact with their surroundings, making it a valuable tool for assessing radio wave propagation in real-world scenarios [36], [37].

We employ a 3D optical ray-tracing method to predict radio wave propagation. This method tracks optical rays from a transmitter to compute propagation loss, considering not only free-space loss but also losses due to penetration, reflection, and diffraction by obstacles. Increasing the number of propagation paths, penetrations, reflections, and diffractions enhances the accuracy of ray-tracing results. However, this also results in longer computation times. To strike a balance between accuracy and computation time, we have configured the ray-tracing parameters, as presented in Table 1. The maximum propagation path, penetrations, reflections, and diffractions for ray-tracing propagation paths are set to 20, 2, 2, and 1, respectively.

Figure 4 shows examples of radio-maps generated by ray-tracing from the different indoor layouts and transmitter positions, illustrating the variation in radio propagation patterns across different settings. The combination of 4800 indoor layouts and 81 transmitter positions generated 388,800 radio-maps, which were divided into 233,280 for training, 77,760 for validating, and 77,760 for testing the deep learning network.

Figure 5 represents the grayscale corresponding to the RSS. In the grayscale, a brighter color indicates a higher RSS, while a darker color represents a lower RSS. It is worth noting that on a practical 2.4 GHz Wi-Fi network, RSS typically ranges from -25 dBm to -100 dBm. An RSS over -26 dBm is represented as RGB (0, 0, 0), and an RSS under -108 dBm is represented as RGB (255, 255, 255).

IV. RADIORESUNET

This section introduces the proposed deep learning network, called RadioResUNet, which is a CNN model for inferring RSS in indoor environments. RadioResUNet comprises two UNet models, namely Front_UNet and Back_UNet, as illustrated in Figure 6. Each UNet model includes an encoder, a decoder, and a bridge, where the encoder downsamples the input image, the decoder upsamples the downsampled image to the same resolution as the input image, and the bridge connects the encoder and the decoder. Additionally, both Front_UNet and Back_UNet feature a skip connection between the encoder and the decoder.

A. INPUT, OUTPUT AND TARGET

The training model requires two grayscale images as input, both of which have a shape of (256, 256, 1): an indoor layout and a transmitter position. It's worth noting that (256, 256, 1) represents (H, W, C), which denotes the image height (H), width (W), and channel (C). These two images are combined to form a single input with a shape of (256, 256, 2). During the recursive training period, the model generates a grayscale radio-map as an output image, which is then compared to a ground truth radio-map serving as the target image selected from the validation dataset. Both the output and target images have the same shape of (256, 256, 1).

B. FRONT_UNET AND BACK_UNET

The Front_UNet, which has bigger filters in both the encoder and decoder, roughly extracts features from the input image, while the Back_UNet, which has smaller filters in both the encoder and decoder, further refines the features from the output of Front_UNet. This results in a more precise representation of the target radio-map. Figure 7 illustrates the predicted outputs from both Front_UNet and Back_UNet, which are compared to the ground truth radio-map. The example demonstrates that Front_UNet estimates the RSS roughly, while Back_UNet estimates it more accurately compared to the ground truth.

C. ENCODER

The encoder of Front_UNet (Encoder$_F$) uses a ResNet structure, as shown in Figure 8, to convolve the input image. This image has been downsampled into a series of feature maps with varying numbers of channels. The feature maps begin at (256, 256, 2) and end at (2, 2, 1000). Encoder$_F$ processes the input image using a recursive sequence of feature map sizes: (256, 256, 2) $\rightarrow$ (128, 128, 40) $\rightarrow$ (64, 64, 60) $\rightarrow$ (32, 32, 100) $\rightarrow$ (16, 16, 150) $\rightarrow$ (8, 8, 300) $\rightarrow$ (4, 4, 500) $\rightarrow$ (2, 2, 1000) as shown in Figure 8 (a).

The encoder of Back_UNet (Encoder$_B$) also has a ResNet structure, similar to that of Front_UNet. It convolves an image created by concatenating the input image and the output image from Front_UNet into a series of feature maps with varying numbers of channels, starting at (256, 256, 3) and ending at (2, 2, 110). Encoder$_B$ processes the input image

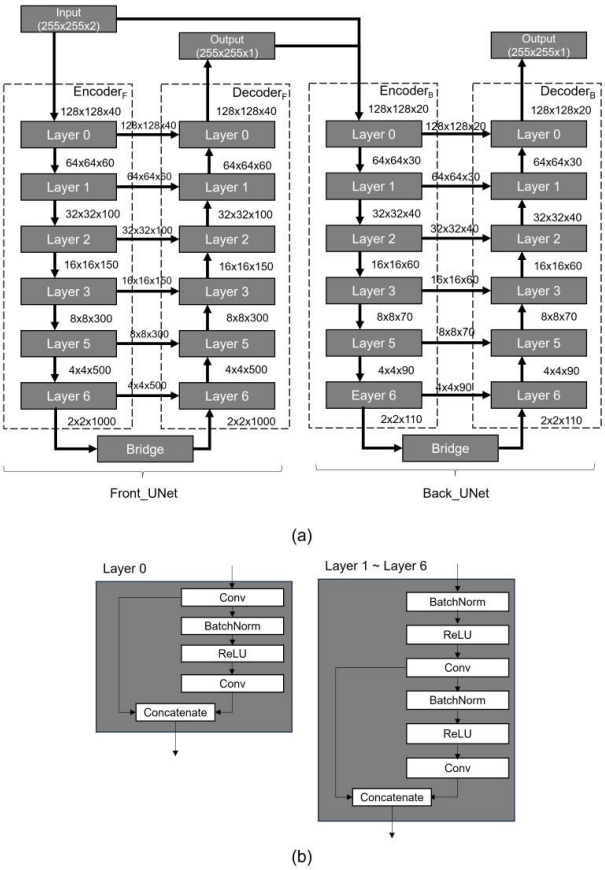

FIGURE 8. A structure of the encoders and the decoders with skip connections of RadioResUNet (a) and ResNet structure for each layer of encoders and decoders (b).

using a recursive sequence of feature map sizes: (256, 256, 3) → (128, 128, 20) → (64, 64, 30) → (32, 32, 40) → (16, 16, 60) → (8, 8, 70) → (4, 4, 90) → (2, 2, 110) as illustrated in Figure 8 (a).

D. DECODER

The decoders of Front_UNet (Decoder$_F$) and Back_UNet (Decoder$_B$) have a ResNet structure similar to those of the encoders, but the decoders are connected to the corresponding encoders through skip connections as shown in Figure 8. The decoders restore the downsampled image to the same resolution as the input image. The skip connection between the encoders and decoders restores the feature map location information lost during encoding.

The decoder of Front_UNet (Decoder$_F$) processes the input image using a recursive sequence of feature map sizes: (2, 2, 1000) → (4, 4, 500) → (8, 8, 300) → (16, 16, 150) → (32, 32, 100) → (64, 64, 60) → (128, 128, 40) → (256, 256, 1). The decoder of Back_UNet (Decoder$_B$) processes the input image using a recursive sequence of feature map sizes: (2, 2, 110) → (4, 4, 90) → (8, 8, 70) →(16, 16, 60) → (32, 32, 40) → (64, 64, 30) → (128, 128, 20) → (256, 256, 1) as illustrated in Figure 8 (a).

E. BRIDGE

The encoder and decoder in each Front_UNet and Back_UNet are connected by a bridge, which serves as a link between the downsampling and upsampling stages. The bridge helps to transfer high-level feature maps from the encoder to the corresponding decoder, enabling the decoder to reconstruct the original input image with greater accuracy.

F. LOSS FUNCTION, OPTIMIZER AND LEARNING RATE

During training of the network, various loss functions such as mean squared error (MSE), binary cross-entropy (BCE), and the combination of dice loss and BCE (Dice_BCE) are applied to optimize the model.

Mean squared error (MSE) loss is

$$MSE = \frac{1}{n}\sum_{i=1}^{n}(\widehat{y}_i - y_i)^2, \tag{1}$$

where n is the number of pixels in the training image, $\widehat{y}$ is the predicted result, and y is the ground truth.

Binary cross-entropy (BCE) loss is

$$BCE = -[y_n log\widehat{y}_n + (1 - y_n)log(1 - \widehat{y}_n)], \tag{2}$$

where n is the number of samples in the dataset, y is the true binary label of {0, 1}, and $\widehat{y}$ is the predicted probability that the label is 1.

Dice binary cross-entropy (Dice_BCE) loss is

$$Dice\_BCE = DL + BCE, \tag{3}$$

where DL is dice loss represented by 1 minus *dice coefficient* (e). Dice coefficient (e) represents the overlap area between ground truth and prediction over the total area of ground truth and prediction.

$$\begin{aligned} DL &= 1 - e \\ &= 1 - \frac{2\sum_{i=1}^{N} y_i\widehat{y}_i + 1}{\sum_{i=1}^{N}(y_i + \widehat{y}_i) + 1}, \end{aligned} \tag{4}$$

where n is the number of pixels in the training image, $\widehat{y}$ is the predicted result, and y is the ground truth.

The adam optimizer is applied with a learning rate of 0.001 using a predefined schedule.

V. RADIO ESTIMATION VERIFICATION

Here, we verify the feasibility and effectiveness of the proposed deep learning-based indoor radio estimation. For this, we compare the RSS obtained from actual measurements by wireless equipment with those obtained by RadioResUNet in two indoor environments: an anechoic chamber and an office floor. Additionally, we investigate the prediction results obtained using different loss functions and varying numbers of datasets. To evaluate the estimation performance, we conduct a comparison between the deep learning-based radio estimation and the empirical channel model of ITU-R P.1238-12 [10]. Finally, we present a radio estimation tool that utilizes the deep learning network of RadioResUNet to predict the wireless environment with minimal information.

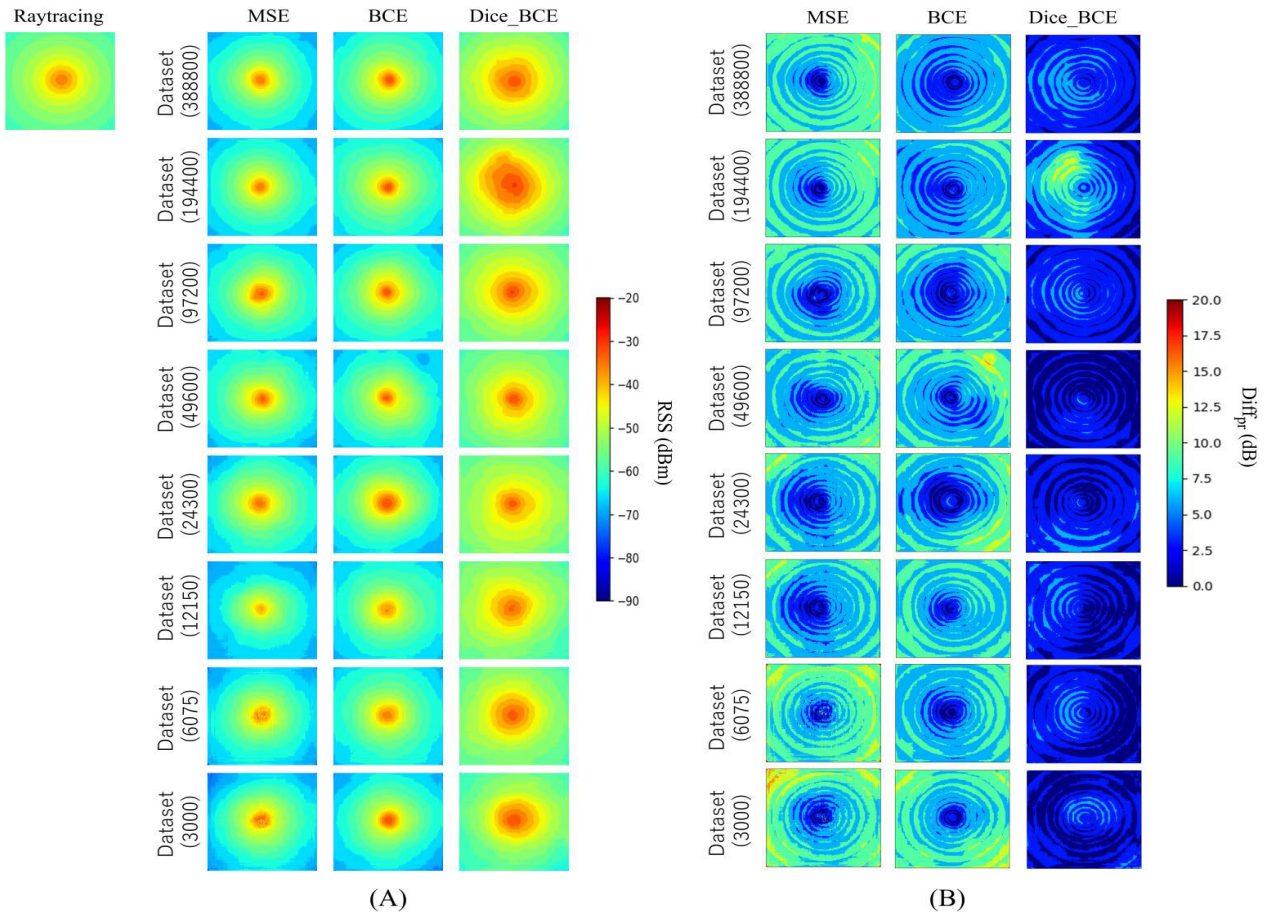

FIGURE 9. Predicted outputs (A) and differences of ray-tracing and predicted RSS (B) upon the loss functions without external interference.

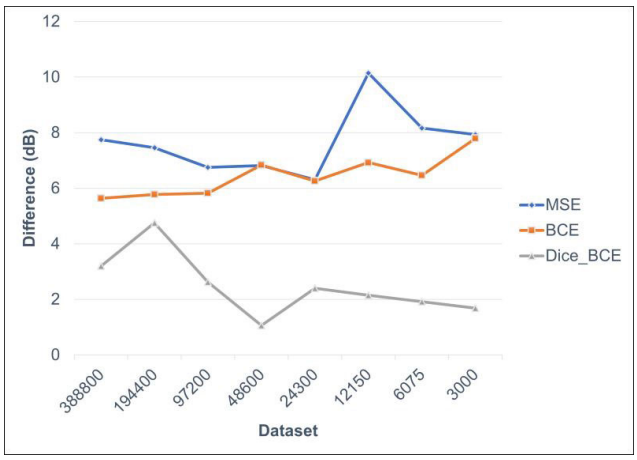

FIGURE 10. Differences of ray-tracing and predicted RSS upon the loss functions and datasets.

Note that the hardware components for deep learning include an NVIDIA RTX 3090 GPU, an Intel i9 processor with a clock speed of 2.8 GHz, and 64 GB of RAM. In addition, we utilize PyTorch and CUDA 11.4 as deep learning frameworks for building and training the deep learning network.

A. PREDICTION VERIFICATION

Figure 9 (A) illustrates the radio estimation results obtained from ray-tracing and the predictions generated by RadioResUNet using the different loss functions and datasets in an environment that mitigates external interference and distortion. Figure 9 (B) shows the disparities between the ray-tracing results and the predictions. Figure 10 depicts the differences between ray-tracing and predictions when changing the number of datasets in each loss function. Note that *difference* ($Diff_{pr}$) is defined as the absolute value of the discrepancy between the predicted RSS (RSS_p) and the ray-traced RSS (RSS_r) at each pixel of the image in all loss functions, represented by:

$$Diff_{pr} = |RSS_p - RSS_r|_i, \tag{5}$$

where i indicates the pixel position of the image of 256 × 256 pixels.

It can be seen that the predictions using Dice_BCE have a lower difference level compared to those using MSE

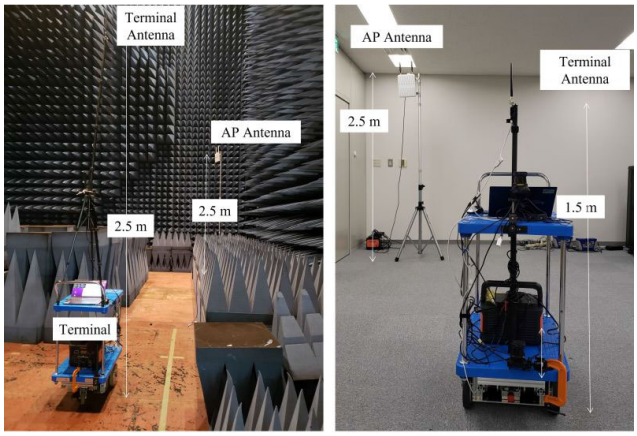

FIGURE 11. Measurement by a driving robot in the anechoic chamber and the office floor.

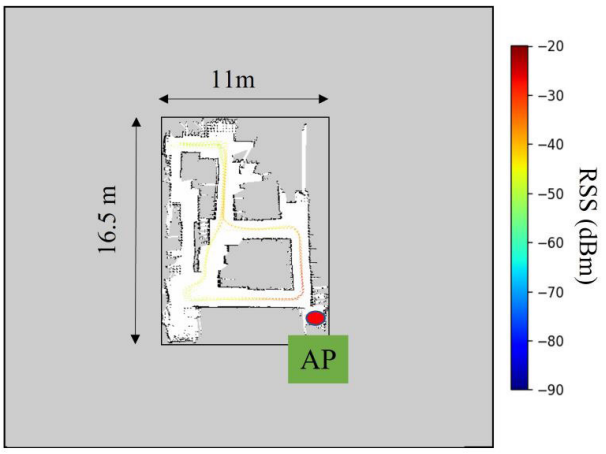

FIGURE 12. Measured RSS by the robot traversing the anechoic chamber.

and BCE. The best difference case for Dice_BCE is 1.06 dB at 48,600 datasets, while those for MSE and BCE are 5.635 dB at 388,800 datasets and 6.301 dB at 24,300 datasets, respectively. These results indicate that RadioResUNet using Dice_BCE provides more accurate prediction results compared to MSE and BCE. Although we do not find a significant difference in prediction when changing the dataset in this case study, we will observe the effect of datasets on radio prediction in practical environments in the following section.

B. PRACTICAL MEASUREMENT ENVIRONMENTS

To verify the feasibility of indoor radio estimation based on deep learning, we conducted a comparison between the radio estimations obtained by RadioResUNet and the practical measurements using wireless equipment taken in an anechoic chamber and an office floor.

Figure 11 shows practical radio measurements conducted in the anechoic chamber and on the office floor. The anechoic chamber was chosen to eliminate external signal interference between a Wi-Fi access point (AP) and a terminal. It has dimensions of 11.1 m × 16.5 m (Figure 11 (a)). The antennas of both the AP and the terminal are positioned at a height of 2.5 m. On the other hand, the office floor provides a larger space of 30 m × 25 m, with the antennas of the AP and the terminal placed at heights of 2.5 m and 1.5 m, respectively (Figure 11 (b)).

We employ an autonomous driving robot to continuously measure RSS between an AP and a mobile terminal within a room. The robot is equipped with simultaneous localization and mapping (SLAM) and navigation functions, utilizing sensor data from a laser range finder (LRF) and map information to estimate its position. The robot can autonomously move from one point to another while recording its position and RSS data [38], [39], [40]. Note that the map and robot position information are used to align the pixel positions of the radio estimation images obtained by RadioResUNet with the practical measurements.

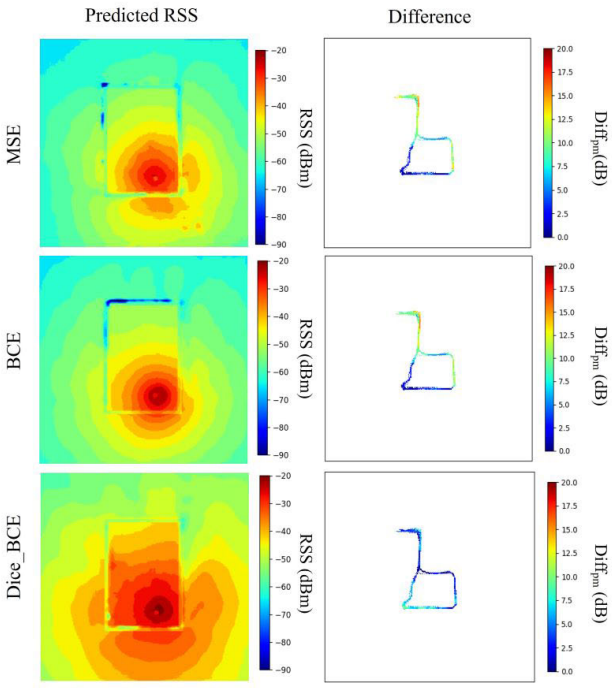

Loss Function	Average Difference
MSE	7.29 dB
BCE	6.20 dB
Dice_BCE	4.25 dB

FIGURE 13. Predicted RSS and differences upon loss functions in the anechoic chamber.

C. ACCURACY IN AN ANECHOIC CHAMBER

Figure 12 provides a visual representation of the RSS measurements obtained as the robot traversed the anechoic chamber, capturing data points across the space. The obtained RSS data is crucial for assessing the performance of the RadioResUNet model. Additionally, Figure 13 presents the RSS predictions generated by RadioResUNet using

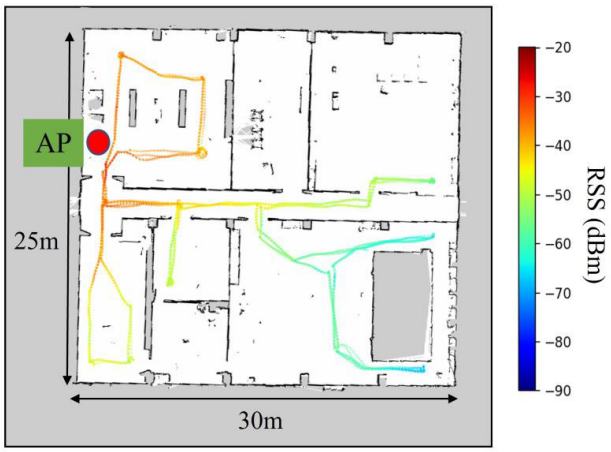

FIGURE 14. Measured RSS by the robot traversing the office floor.

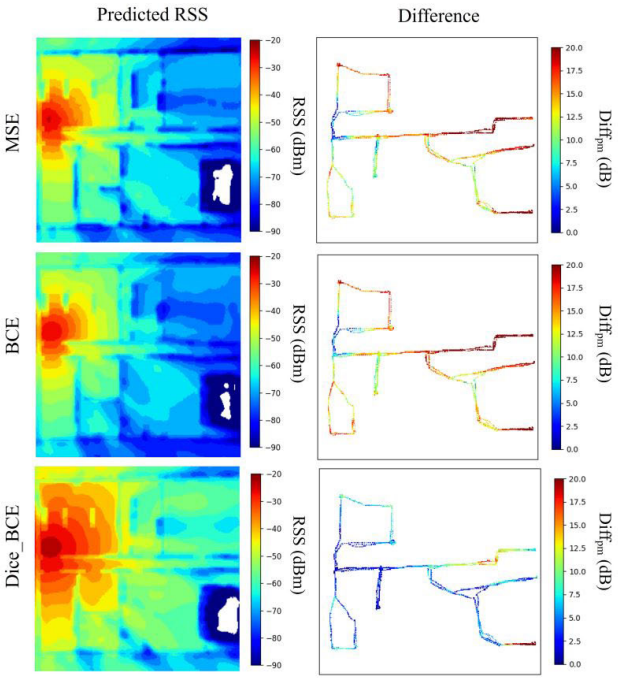

Loss Function	Average Difference
MSE	12.69 dB
BCE	13.31 dB
Dice_BCE	5.40 dB

FIGURE 15. Predicted RSS and differences upon loss functions in the office floor.

three distinct loss functions: MSE, BCE, and Dice_BCE. These figures also illustrate the differences between these predicted RSS values and the actual measurements, offering a comprehensive view of the model's accuracy under various loss functions. Note that *difference* ($Diff_{pm}$) is defined as the absolute value of the discrepancy between the predicted RSS (RSS_p) and the robot measured RSS (RSS_m) at each pixel of

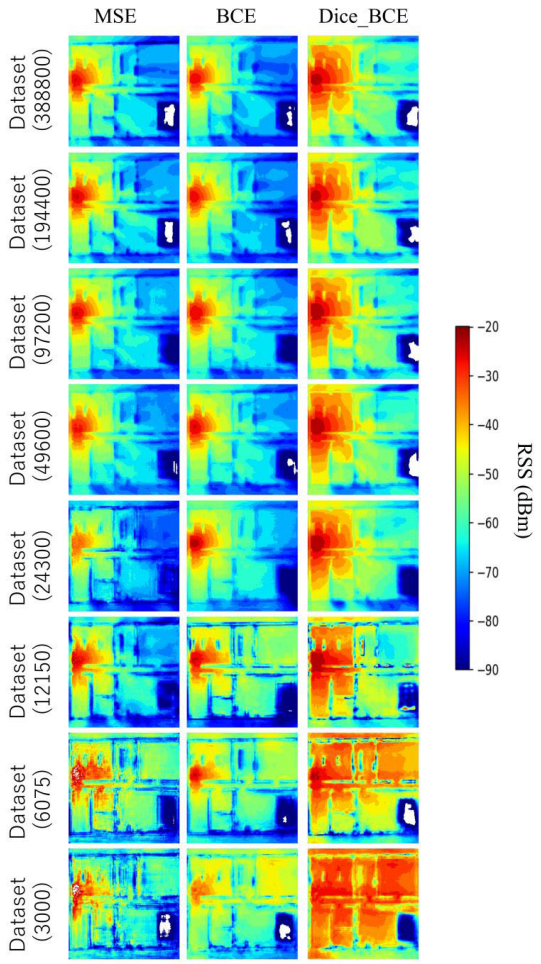

FIGURE 16. Predicted RSS upon changing datasets corresponding to loss functions in the office floor.

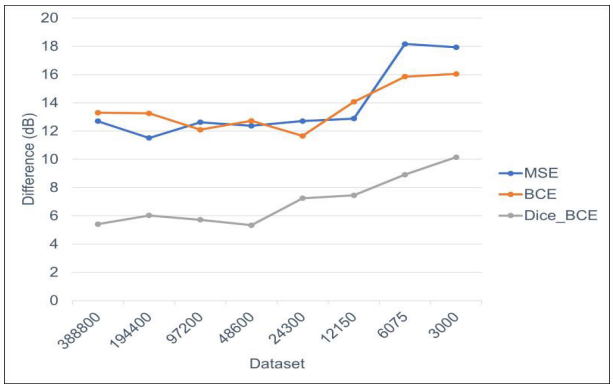

FIGURE 17. Average differences between the robot measurement and the predictions upon changing datasets.

the image in all loss functions, represented by:

$$Diff_{pm} = |RSS_p - RSS_m|_i, \tag{6}$$

where i indicates the pixel position of the image of 256 × 256 pixels.

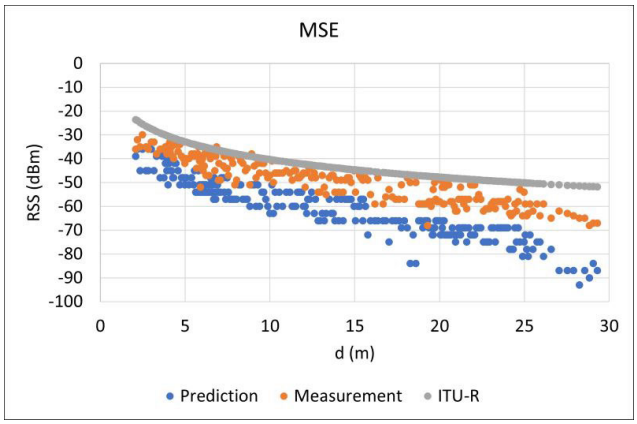

FIGURE 18. RSSs upon changing the separation distance between AP and terminal (d) estimated by the deep learning prediction of MSE, robot measurement, and ITU-R P.1238 indoor channel model.

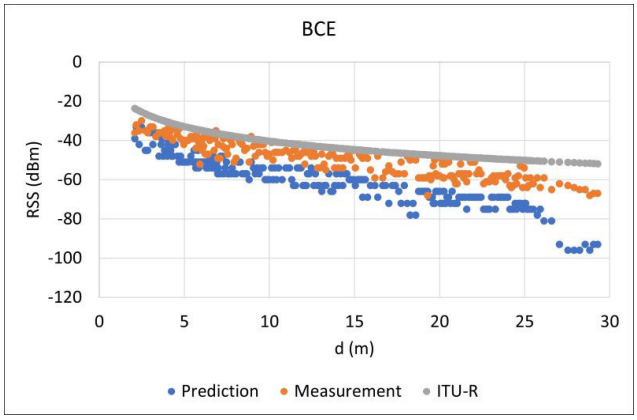

FIGURE 19. RSSs upon changing the separation distance between AP and terminal (d) estimated by the deep learning prediction of BCE, robot measurement, and ITU-R P.1238 indoor channel model.

The average RSS differences for MSE, BCE, and Dice_BCE are 7.29 dB, 6.20 dB, and 4.25 dB, respectively. The Dice_BCE loss function provides higher accuracy compared to MSE and BCE.

D. ACCURACY IN AN OFFICE FLOOR

Figure 14 provides a visual representation of RSS as measured by the robot traversed the office floor, capturing data points across the space. Figure 15 displays the RSS predictions generated by RadioResUNet using three distinct loss functions: MSE, BCE, and Dice_BCE. The accompanying figures also present the differences between these predicted RSS values and the actual measurements, providing a comprehensive view of the model's accuracy under different loss functions. On average, the RSS differences for MSE, BCE, and Dice_BCE stand at 12.69 dB, 13.30 dB, and 5.40 dB, respectively. Notably, the Dice_BCE loss function yields higher accuracy when compared to MSE and BCE.

E. ACCURACY UPON CHANGING DATASETS

Figure 16 offers valuable insights into the predicted RSS across a range of dataset sizes. These datasets encompass various sizes, with data points collected from 388,800 to 3,000 samples. The predictions are generated using distinct loss functions, including MSE, BCE, and Dice_BCE. In conjunction with this, Figure 17 complements the understanding by representing the average RSS differences observed as the dataset size varies, with a specific focus on the performance under each loss function. It's noteworthy that the Dice_BCE loss function demonstrates an advantage in terms of prediction accuracy when compared to MSE and BCE.

Furthermore, a key observation arises when delving into the dataset size dynamics. Particularly, it becomes evident that prediction accuracy generally exhibits a decline when operating with smaller datasets, which is especially pronounced at the 24,300 dataset size. This illustrates the sensitivity of the model's performance to dataset size. However, it's worth noting that beyond this point, a substantial increase in dataset size does not yield a significant enhancement in prediction accuracy.

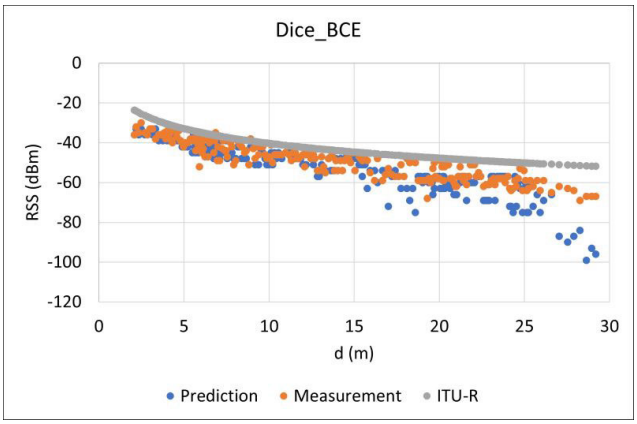

FIGURE 20. RSSs upon changing the separation distance between AP and terminal (d) estimated by the deep learning prediction of Dice_BCE, robot measurement, and ITU-R P.1238 indoor channel model.

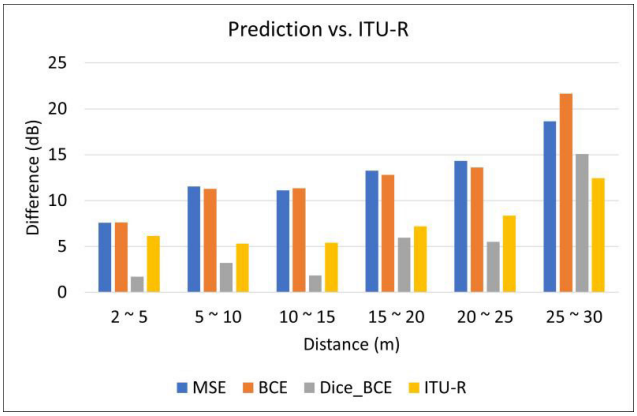

FIGURE 21. Comparison of the estimation differences between each deep learning prediction of MSE, BCE, and Dice_BCE and robot measurement and between ITU-R P.1238 and robot measurement.

F. PERFORMANCE COMPARED TO ITU-R P.1238 INDOOR CHANNEL MODEL

To evaluate the estimation performance, we conduct a comparison between the deep learning-based predictions and the empirical channel model of ITU-R P.1238-12 [10]. ITU-R P.1238-12 provides recommendations for propagation data and prediction methods for the planning of indoor radiocommunication systems and radio local area networks in the frequency range 300 MHz to 450 GHz.

The basic transmission loss model of ITU-R P.1238-12 has the following form:

$$L = 10\alpha log_{10}(d) + \beta + 10\gamma log_{10}(f) \tag{7}$$

d represents the separation distance in meters between the AP and terminal, f represents frequency in GHz, α represents the coefficient of distance transmission loss, β represents the coefficient offset value of the basic transmission loss, γ represents the coefficient of frequency transmission loss. For an office non-line of sight (NLOS) environment on the same floor, the parameters are set as follows: $f = 2.44$, $\alpha = 2.46$, $\beta = 29.53$, and $\gamma = 2.38$.

Figures 18, 19, and 20 present detailed results illustrating how RSS changes with variations in the separation distance (d) between the access point (AP) and the terminal. These figures display results obtained from three sources: robot measurements, the ITU-R P.1238 indoor channel model, and the deep learning predictions using MSE, BCE, and Dice_BCE, respectively.

In addition to these individual representations, Figure 21 provides a comprehensive overview of the estimation differences. It compares the RSS predictions made by the deep learning models (using MSE, BCE, and Dice_BCE) with the RSS measurements obtained from the robot. It also contrasts the RSS predictions generated by the ITU-R P.1238 indoor channel model with the robot's RSS measurements.

Remarkably, the results show that the deep learning-based predictions using the Dice_BCE loss function offer performance on par with or exceeding that of the predictions generated by the ITU-R indoor channel model for separation distances up to 25 meters.

G. PERFORMANCE UPON CHANGING IMAGE SIZE

We have conducted a comprehensive analysis to assess the relationship between training image size and its impact on our deep learning outcomes. Training image size can potentially influence various aspects, including computational processing time and the performance of prediction results.

The results, labeled as (a), (b), and (c) in Figure 22, depict the training time per epoch and RSS estimation results when altering the input image size to 128 × 128, 256 × 256, and 512 × 512, respectively. Notably, using a 512 × 512 input image requires approximately 1100 seconds for Front_UNet and around 860 seconds for Back_UNet. A 256 × 256 input image takes roughly 360 seconds for Front_UNet and about 290 seconds for Back_UNet, while a 128 × 128 input image consumes approximately 240 seconds for Front_UNet and around 215 seconds for Back_UNet. Intuitively, larger images demand longer processing times due to the increased number of pixels to train, and vice versa.

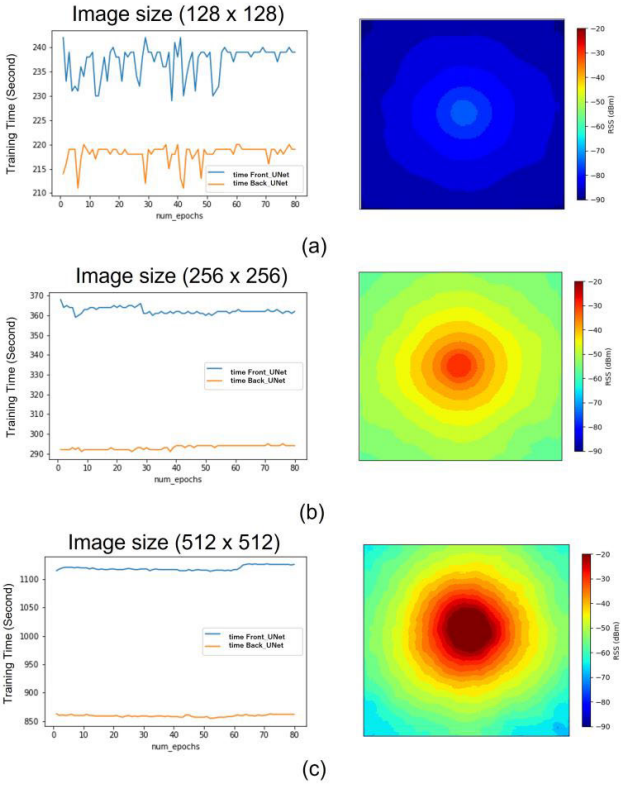

FIGURE 22. Training time and RSS prediction result upon changing learning image size of 128 x 128, 256 x 256, and 512 x 512.

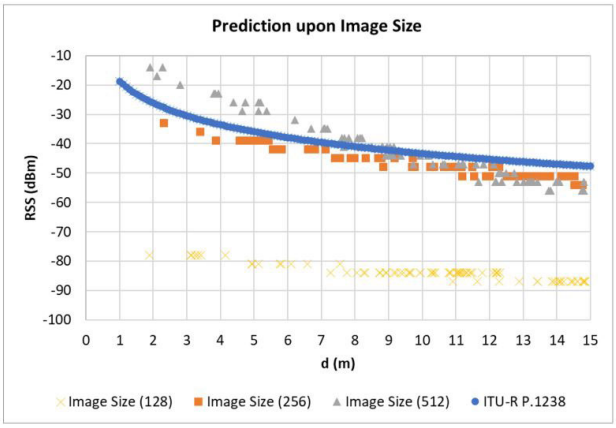

FIGURE 23. RSSs upon changing the image size for the deep learning prediction.

Figure 23 illustrates that employing a larger image size of 512 × 512 does not improve RSS prediction compared to the 256 × 256 image size. On the contrary, when the distance is less than 7 meters, the image size of 256 × 256 provides a prediction result closer to that of 512 × 512, as compared to the RSS prediction of ITU-R. On the other hand, a smaller image size of 128 × 128 leads to a noticeable decrease in

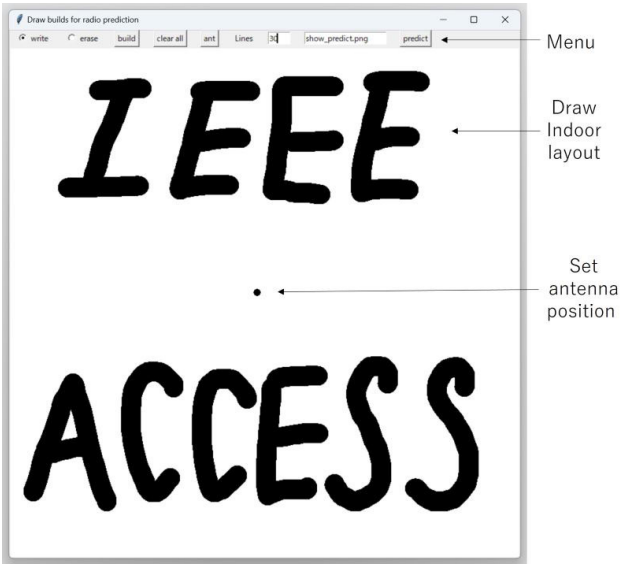

FIGURE 24. A radio propagation estimation tool for drawing an indoor layout.

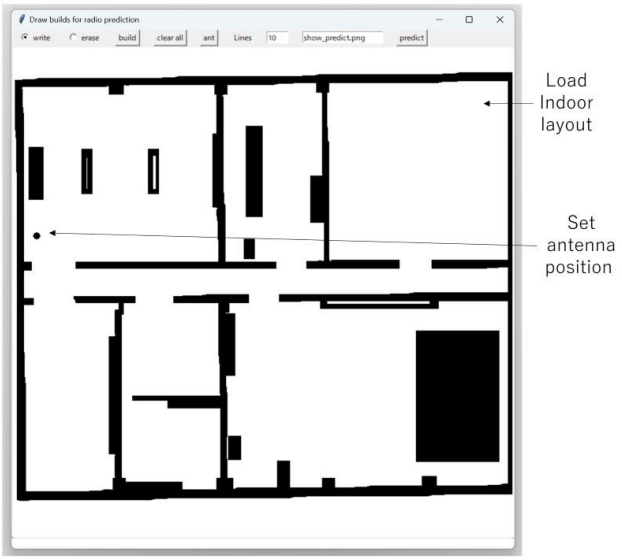

FIGURE 26. A radio propagation estimation tool for loading an indoor layout.

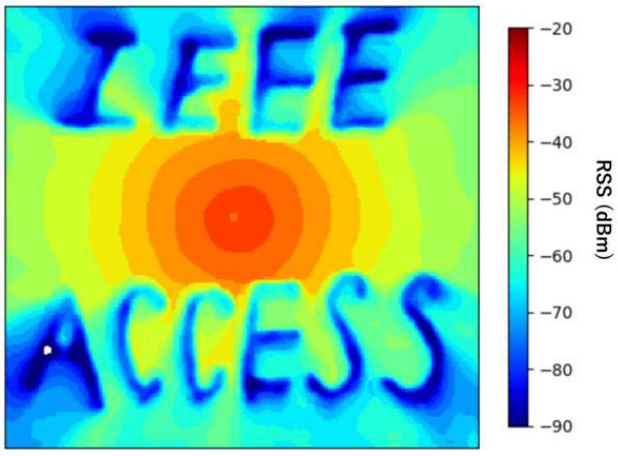

FIGURE 25. A radio propagation estimation output.

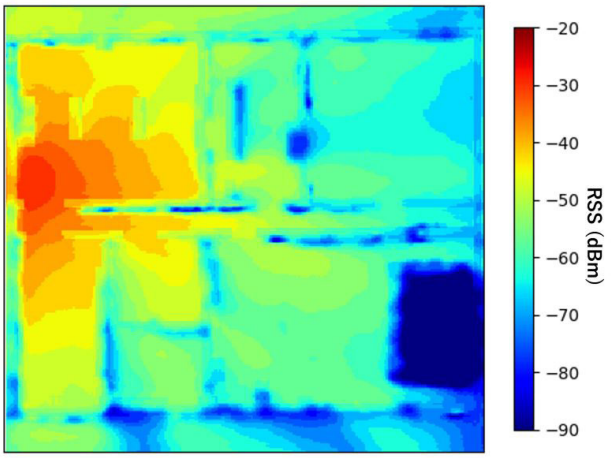

FIGURE 27. A radio propagation estimation output.

performance compared to the 256 × 256 image size, even though it reduces computational processing time. The results demonstrate that choosing the appropriate image size is a crucial aspect of deep learning for radio estimation using CNNs, and an image size of 256 × 256 strikes a good balance between prediction accuracy and computational processing time.

H. A RADIO PROPAGATION ESTIMATION TOOL

We have developed a user-friendly radio estimation tool that utilizes deep learning to predict the radio environment in a targeted area with minimal input. Unlike traditional approaches that require analytical models and simulation expertise, the tool simplifies the process of deploying wireless networks, making it accessible even for beginners.

The tool's interface, as shown in Figure 24 and Figure 26, includes a menu and canvas that enable users to draw or load the indoor layout and to set the position of the antenna. With just two inputs - the indoor layout and the antenna position - the tool generates a predicted radio propagation of RSS, as depicted in Figure 25 and Figure 27. By simplifying the measurement process and removing the requirement for analytical models, the tool streamlines the wireless network deployment procedure and enables users to concentrate on the practical aspects of wireless network implementation.

VI. CONCLUSION

This paper introduced a novel approach for estimating indoor radio propagation using deep learning. Our method leveraged a training dataset comprising diverse real-world indoor environments and radio-map images generated through ray-tracing radio propagation. We introduced a convolutional neural network (CNN) called RadioResUNet, which played a pivotal role in training and predicting indoor

radio environments. The feasibility and effectiveness of the deep learning-based indoor radio estimation were validated through a meticulous comparison of RSS obtained through practical measurements and that obtained using RadioResUNet. Our assessment covered two indoor environments: an anechoic chamber and an office floor. Moreover, we explored the prediction outcomes obtained using different loss functions of MSE, BCE, and Dice_BCE and varying dataset sizes. The results indicated that our deep learning-based radio estimation method achieved measurement discrepancies of 4.25 dB and 5.4 dB compared to practical measurements carried out by an automatic driving robot with wireless equipment in real-world environments of the anechoic chamber and the office floor, respectively. The outcomes implied that our prediction performance was comparable to the indoor channel model of ITU-R P.1238. Lastly, we introduced a user-friendly radio estimation tool that harnessed deep learning to predict the radio environment in a specific area with minimal input.

The proposed recursive network structure of Front_UNet and Back_UNet could operating quasi-tuning in Front_UNet and fine-tuning in Back_UNet. This investigation has raised an important question concerning the optimal number of iterative UNet operations to achieve peak performance. Our forthcoming research will focus on enhancing our approach by meticulously reconstructing UNet, taking into account convolutional and optimization parameters. Furthermore, to enable a broader application of deep learning-based radio estimation in wireless communications, several factors need to be considered in future work:

- Antenna Types: With wireless systems evolving to achieve higher throughput and improved radio access, various antenna types like MIMO (Multiple Input, Multiple Output) and beamforming antennas are being adopted.
- Operational Frequencies: In addition to current wireless communication frequencies, the wireless communication landscape is expanding to encompass a wider range of frequencies. This includes the utilization of new radio frequencies such as millimeter-wave and terahertz in future wireless communication technologies.
- Wireless Environments: Recognizing the significant differences in radio propagation characteristics between indoor and outdoor environments is crucial. Furthermore, it's essential to consider extreme areas such as tunnels, deep-sea environments, and outer space as potential scenarios for future wireless communication.

NOTATION

Following abbreviations and symbols are used in this paper:

BCE	Binary Cross-Entropy.
CNN	Convolutional Neural Network.
Dice_BCE	Dice Binary Cross-Entropy.
MSE	Mean Squared Error.
ResUNet	Residual UNet.
RadioResUNet	Radio Residual UNet.
RSS	Received Signal Strength.
d	distance between a transmitter and a receiver.
f	operation frequency (GHz).
α	coefficient of distance transmission loss.
β	coefficient of the offset of basic transmission loss.
γ	coefficient of frequency transmission loss.

REFERENCES

[1] R. Khatoun and S. Zeadally, "Smart cities: Concepts, architectures, research opportunities," *Commun. ACM*, vol. 59, no. 8, pp. 46–57, Jul. 2016.

[2] N. K. Jha, "Smart healthcare," in *Proc. IEEE Int. Conf. Consum. Electron. (ICCE)*, Las Vegas, NV, USA, Jan. 2018, p. 1, doi: 10.1109/ICCE.2018.8326054.

[3] *Family of Standards for Wireless Access in Vehicular Environments (WAVE)*, Standard IEEE 1609, Apr. 2013.

[4] B. Chen, J. Wan, L. Shu, P. Li, M. Mukherjee, and B. Yin, "Smart factory of industry 4.0: Key technologies, application case, and challenges," *IEEE Access*, vol. 6, pp. 6505–6519, 2018, doi: 10.1109/ACCESS.2017.2783682.

[5] *Beyond 5G/6G White Paper*. Accessed: 2023. [Online]. Available: https://beyond5g.nict.go.jp/download/index.html

[6] I. F. Akyildiz, A. Kak, and S. Nie, "6G and beyond: The future of wireless communications systems," *IEEE Access*, vol. 8, pp. 133995–134030, 2020, doi: 10.1109/ACCESS.2020.3010896.

[7] K. Haneda, R. Rudd, E. Vitucci, D. He, P. Kysti, F. Tufvesson, S. Salous, Y. Miao, W. Joseph, and E. Tanghe, "Radio propagation modeling methods and tools," in *Inclusive Radio Communications for 5G and Beyond*. New York, NY, USA: Academic, 2021.

[8] T. Matsumura, H. Sawada, T. Miyachi, F. Kojima, H. Harai, A. Sakaguchi, Y. Nishigori, and H. Harada, "Development and initial implementation of large-scale wireless emulator toward beyond 5G," in *Proc. 25th Int. Symp. Wireless Pers. Multimedia Commun. (WPMC)*, Herning, Denmark, Oct. 2022, pp. 199–204, doi: 10.1109/WPMC55625.2022.10014899.

[9] T. Matsumura and H. Sawada, "Investigation of beyond 5G-based physical radio node emulation for large-scale wireless emulator," in *Proc. 25th Int. Symp. Wireless Pers. Multimedia Commun. (WPMC)*, Herning, Denmark, Oct. 2022, pp. 400–405, doi: 10.1109/WPMC55625.2022.10014875.

[10] *Propagation Data and Prediction Methods for the Planning of Indoor Radiocommunication Systems and Radio Local Area Networks in the Frequency Range 300 MHz to 450 GHz*, document ITU-R P.1238-12, 2023.

[11] Q. Mao, F. Hu, and Q. Hao, "Deep learning for intelligent wireless networks: A comprehensive survey," *IEEE Commun. Surveys Tuts.*, vol. 20, no. 4, pp. 2595–2621, 4th Quart., 2018, doi: 10.1109/COMST.2018.2846401.

[12] T. O'Shea and J. Hoydis, "An introduction to deep learning for the physical layer," *IEEE Trans. Cognit. Commun. Netw.*, vol. 3, no. 4, pp. 563–575, Dec. 2017, doi: 10.1109/TCCN.2017.2758370.

[13] Z. Qin, H. Ye, G. Y. Li, and B. F. Juang, "Deep learning in physical layer communications," *IEEE Wireless Commun.*, vol. 26, no. 2, pp. 93–99, Apr. 2019, doi: 10.1109/MWC.2019.1800601.

[14] H. Huang, S. Guo, G. Gui, Z. Yang, J. Zhang, H. Sari, and F. Adachi, "Deep learning for physical-layer 5G wireless techniques: Opportunities, challenges and solutions," *IEEE Wireless Commun.*, vol. 27, no. 1, pp. 214–222, Feb. 2020, doi: 10.1109/MWC.2019.1900027.

[15] T. Ohtsuki, "Machine learning in 6G wireless communications," *IEICE Trans. Commun.*, vol. 106, no. 2, pp. 75–83, 2023.

[16] B. Zhu, J. Wang, L. He, and J. Song, "Joint transceiver optimization for wireless communication PHY using neural network," *IEEE J. Sel. Areas Commun.*, vol. 37, no. 6, pp. 1364–1373, Jun. 2019, doi: 10.1109/JSAC.2019.2904361.

[17] S. K. Goudos, G. V. Tsoulos, and G. Athanasiadou, "Modelling received signal power in modern mobile communications with UAVs using ensemble learning," in *Proc. 13th Eur. Conf. Antennas Propag. (EuCAP)*, Krakow, Poland, Mar. 2019, pp. 1–4.

[18] L. Liang, H. Ye, G. Yu, and G. Y. Li, "Deep-learning-based wireless resource allocation with application to vehicular networks," *Proc. IEEE*, vol. 108, no. 2, pp. 341–356, Feb. 2020, doi: 10.1109/JPROC.2019.2957798.

[19] Y. Yu, T. Wang, and S. C. Liew, "Deep-reinforcement learning multiple access for heterogeneous wireless networks," in *Proc. IEEE Int. Conf. Commun. (ICC)*, May 2018, pp. 1–7.

[20] E. Ghadimi, F. D. Calabrese, G. Peters, and P. Soldati, "A reinforcement learning approach to power control and rate adaptation in cellular networks," in *Proc. IEEE Int. Conf. Commun. (ICC)*, May 2017, pp. 1–7.

[21] Z. Li, X. Wang, L. Pan, L. Zhu, Z. Wang, J. Feng, C. Deng, and L. Huang, "Network topology optimization via deep reinforcement learning," *IEEE Trans. Commun.*, vol. 71, no. 5, pp. 2847–2859, May 2023, doi: 10.1109/TCOMM.2023.3244239.

[22] G. Nguyen, S. Dlugolinsky, V. Tran, and Á. López García, "Deep learning for proactive network monitoring and security protection," *IEEE Access*, vol. 8, pp. 19696–19716, 2020, doi: 10.1109/ACCESS.2020.2968718.

[23] T. Wong, G. Chan, and F. Chua, "A machine learning model for detection and prediction of cloud quality of service violation," in *Proc. ICCSA*, in Lecture Notes in Computer Science, vol. 10960. Cham, Switzerland: Springer, 2018, pp. 498–513.

[24] W. Cui, K. Shen, and W. Yu, "Spatial deep learning for wireless scheduling," *IEEE J. Sel. Areas Commun.*, vol. 37, no. 6, pp. 1248–1261, Jun. 2019.

[25] S. Park, Y. Yoo, and C.-W. Pyo, "Applying DQN solutions in fog-based vehicular networks: Scheduling, caching, and collision control," *Veh. Commun.*, vol. 33, Jan. 2022, Art. no. 100397.

[26] L. Liang, H. Ye, and G. Y. Li, "Spectrum sharing in vehicular networks based on multi-agent reinforcement learning," *IEEE J. Sel. Areas Commun.*, vol. 37, no. 10, pp. 2282–2292, Oct. 2019.

[27] J. Reis, M. Rocha, T. K. Phan, D. Griffin, F. Le, and M. Rio, "Deep neural networks for network routing," in *Proc. Int. Joint Conf. Neural Netw. (IJCNN)*, Budapest, Hungary, Jul. 2019, pp. 1–8, doi: 10.1109/IJCNN.2019.8851733.

[28] N. Aloysius and M. Geetha, "A review on deep convolutional neural networks," in *Proc. Int. Conf. Commun. Signal Process. (ICCSP)*, Chennai, India, Apr. 2017, pp. 0588–0592, doi: 10.1109/ICCSP.2017.8286426.

[29] Z. Li, F. Liu, W. Yang, S. Peng, and J. Zhou, "A survey of convolutional neural networks: Analysis, applications, and prospects," *IEEE Trans. Neural Netw. Learn. Syst.*, vol. 33, no. 12, pp. 6999–7019, Dec. 2022, doi: 10.1109/TNNLS.2021.3084827.

[30] K. He, X. Zhang, S. Ren, and J. Sun, "Deep residual learning for image recognition," in *Proc. IEEE Conf. Comput. Vis. Pattern Recognit. (CVPR)*, Jun. 2016, pp. 770–778, doi: 10.1109/CVPR.2016.90.

[31] O. Ronneberger, P. Fischer, and T. Brox, "U-Net: Convolutional networks for biomedical image segmentation," in *Proc. Int. Conf. Med. Image Comput. Comput.-Assist. Intervent.*, 2015, pp. 234–241.

[32] Z. Zhang, Q. Liu, and Y. Wang, "Road extraction by deep residual U-Net," *IEEE Geosci. Remote Sens. Lett.*, vol. 15, no. 5, pp. 749–753, May 2018, doi: 10.1109/LGRS.2018.2802944.

[33] R. Levie, Ç. Yapar, G. Kutyniok, and G. Caire, "RadioUNet: Fast radio map estimation with convolutional neural networks," *IEEE Trans. Wireless Commun.*, vol. 20, no. 6, pp. 4001–4015, Jun. 2021, doi: 10.1109/TWC.2021.3054977.

[34] U. Masood, H. Farooq, and A. Imran, "A machine learning based 3D propagation model for intelligent future cellular networks," in *Proc. IEEE Global Commun. Conf. (GLOBECOM)*, Waikoloa, HI, USA, Dec. 2019, pp. 1–6.

[35] R. Hoppe, G. Wölfle, and U. Jakobus, "Wave propagation and radio network planning software WinProp added to the electromagnetic solver package FEKO," in *Proc. Int. Appl. Comput. Electromagn. Soc. Symp. (ACES)*, Firenze, Italy, Mar. 2017, pp. 1–2, doi: 10.23919/ROPACES.2017.7916282.

[36] T. K. Geok, F. Hossain, and A. T. W. Chiat, "A novel 3D ray launching technique for radio propagation prediction in indoor environments," *PLoS ONE*, vol. 13, no. 8, Aug. 2018, Art. no. e0201905, doi: 10.1371/journal.pone.0201905.

[37] T. K. Geok, F. Hossain, S. K. A. Rahim, O. Elijah, A. A. Eteng, C. T. Loh, L. Li Li, C. P. Tso, T. A. Rahman, and M. N. Hindia, "3D RT adaptive path sensing method: RSSI modelling validation at 4.5 GHz, 28 GHz, and 38 GHz," *Alexandria Eng. J.*, vol. 61, no. 12, pp. 11041–11061, Dec. 2022.

[38] H. Durrant-Whyte and T. Bailey, "Simultaneous localization and mapping (SLAM): Part I, *IEEE Robot. Autom. Mag.*, vol. 13, no. 3, pp. 99–108, Jun. 2006.

[39] T. Bailey and H. Durrant-Whyte, "Simultaneous localization and mapping (SLAM): Part II, *IEEE Robot. Autom. Mag.*, vol. 13, no. 3, pp. 108–117, Sep. 2006.

[40] C.-W. Pyo, H. Sawada, and T. Matsumura, "Experimental study of dynamic data traffic control for the cooperating system of smart personal mobility and indoor intelligent infrastructure," in *Proc. 24th Int. Symp. Wireless Pers. Multimedia Commun. (WPMC)*, Dec. 2021, pp. 1–6, doi: 10.1109/WPMC52694.2021.9700451.

CHANGWOO PYO received the B.E. degree in computer engineering from Youngnam University, South Korea, in 1999, and the M.E. and D.E. degrees in computer sciences from Tsukuba University, Tsukuba, Japan, in 2002 and 2005, respectively. Since he joined the National Institute of Information and Communications Technology (NICT), in 2005, he has been engaged in research on wireless and mobile communications on heterogeneous networks. In current, he works on the MAC protocol design for wireless local area networks (WLAN), wireless personal communication networks (WPAN) on millimeter wave, and beyond 5G and 6G.

HIROKAZU SAWADA (Member, IEEE) received the B.E., M.E., and Ph.D. degrees in electrical and electronic engineering from Gifu University, Japan, in 1997, 1999, and 2002, respectively. From 2002 to 2005, he was a Researcher with the Tohoku Institute of Technology, Japan. From 2005 to 2007, he was an Expert Researcher with the National Institute of Information and Communications Technology (NICT), Japan. From 2007 to 2009, he was a Lecturer with the Tohoku Institute of Technology. From 2009 to 2013, he was an Assistant Professor with the Research Institute of Electrical Communications (RIEC), Tohoku University, Japan. Since 2013, he has been a Researcher and currently a Research Manager with NICT.

TAKESHI MATSUMURA (Member, IEEE) received the M.S. degree in electronic engineering and the Ph.D. degree in nano-mechanics engineering from Tohoku University, Sendai, Japan, in 1998 and 2010, respectively. From 1998 to 2007, he had been engaged in the research and development of wireless communications devices in some companies. In April 2007, he joined the National Institute of Information and Communications Technology (NICT), Tokyo, Japan, as a Researcher with the Smart Wireless Laboratory and engaged in the white-space communication systems and fifth generation mobile communication systems. From April 2016 to March 2019, he was an Associate Professor with the Graduate School of Informatics, Kyoto University, Kyoto, Japan. He is currently the Director of the Wireless Systems Laboratory, NICT, and a Researcher with the Graduate School of Informatics, Kyoto University. His research interests include whitespace communication systems, wide-area wireless network systems, beyond 5G mobile communication systems, and wireless emulation technologies.